Electronic Supplementary Material (ESI) for Materials Advances.
This journal is © The Royal Society of Chemistry 2021

Electronic Supplementary Information

First demonstration of the use of open-shell derivatives as organic luminophores for transparent luminescent solar concentrators

Sara Mattiello,[a] Francesca Corsini,[b] Sara Mecca,[a] Mauro Sassi,[a] Riccardo Ruffo,[a] Giuseppe Mattioli,[c] Yohei Hattori,[d] Tetsuro Kusamoto,[e,]* Gianmarco Griffini[b,]* and Luca Beverina[a,]*

[a] Department of Materials Science, University of Milano-Bicocca, Via R. Cozzi, 55, Milano, Italy.
[b] Department of Chemistry Materials and Chemical Engineering “Giulio Natta”, Politecnico di Milano, Piazza Leonardo da Vinci 32, 20133 Milano, Italy.
[c] CNR - Istituto di Struttura della Materia, Area della Ricerca di Roma, I-00015 Monterotondo Scalo, Italy.
[d] Faculty of Advanced Science and Technology, Ryukoku University, Kyoto, Japan
[e] Department of Life and Coordination-Complex Molecular Science, Institute for Molecular Science, 5-1 Higashiyama, Myodaiji, Okazaki, Aichi 444-8787, Japan

Table of Contents

S1. Synthesis and characterization of new derivatives

Materials and methods

Reagents were bought from Fluorochem, Sigma-Aldrich and Alfa-Aesar. Catalysts were bought from Fluorochem. Solvents were bought from Sigma-Aldrich. Water used as reaction medium was HPLC grade, while deionized water was used during purifications.

Unless otherwise stated, all reagents and solvents were used as received.

NMR spectra were collected with a Bruker NMR Avance 400 NEO.

ESR spectra were recorded with a JEOL JES-FR30EX spectrometer with X-band microwave. Sample solutions were charged in a 5 mm diameter sample tube. Magnetic field was calibrated with the Mn^{2+}/MgO standard. ESR spectra were measured in cyclohexane, and the *g* factors of all the radicals were 2.003.

Synthesis of PyBTM-H

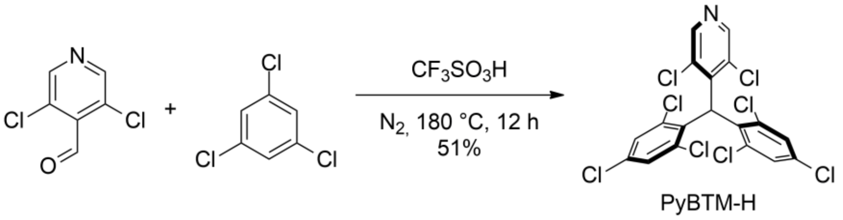

Reaction was performed according to literature conditions.[1]

In a 250 mL roundbottom flask, 3,5-dichloropyridine-4-carboxaldehyde (6.000 g, 34.09 mmol) and 1,3,5-trichlorobenzene (60.60 g, 334.0 mmol) are put under nitrogen atmosphere and melt at 180 °C. Trifluoromethanesulfonic acid (100.00 g, 666.31 mmol) is slowly added, and the mixture is kept stirring at 180 °C for 12 hours. The mixture is subsequently cooled down to room temperature and diluted with CH_2Cl_2 (300 mL). Aqueous 10% NaOH is carefully added until neutral pH, then $NaHCO_3$ is added until the aqueous phase reaches pH=10. The organic phase is extracted, then washed with aqueous $NaHCO_3$, and dried over Na_2SO_4. Organic solvent is evaporated under reduced pressure, and the raw is purified by column chromatography (eluent: CH_2Cl_2/heptane 1:1) to afford the product in the form of a white powder. 9.060 g, 51% yield.

^1H NMR (400 MHz, $CDCl_3$): δ 8.49 (s, 1H), 8.36 (s, 1H), 7.39 (d, J=2.2 Hz, 1H), 7.38 (d, J=2.2 Hz, 1H), 7.27 (d, J=2.2 Hz, 1H), 7.24 (d, J=2.2 Hz, 1H), 6.69 (s, 1H).

Screening of conditions for the synthesis of PyPBTM-H

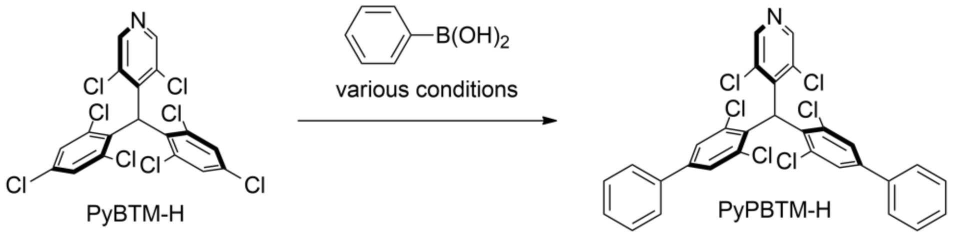

Whenever product formation was observed by TLC (eluent: heptane/CH_2Cl_2 2:1, rf=0.33), the reaction was purified either by column chromatography (eluent: heptane/CH_2Cl_2 2:1) or crystallization (solvent: MeOH/H_2O).

Several conditions were tested to synthesize PyPBTM-H from PyBTM-H, which are summarized in Table 1 of the main text. All the reactions were monitored for 24 hours before workup. Scheme S1 shows the structures of all tested surfactants.

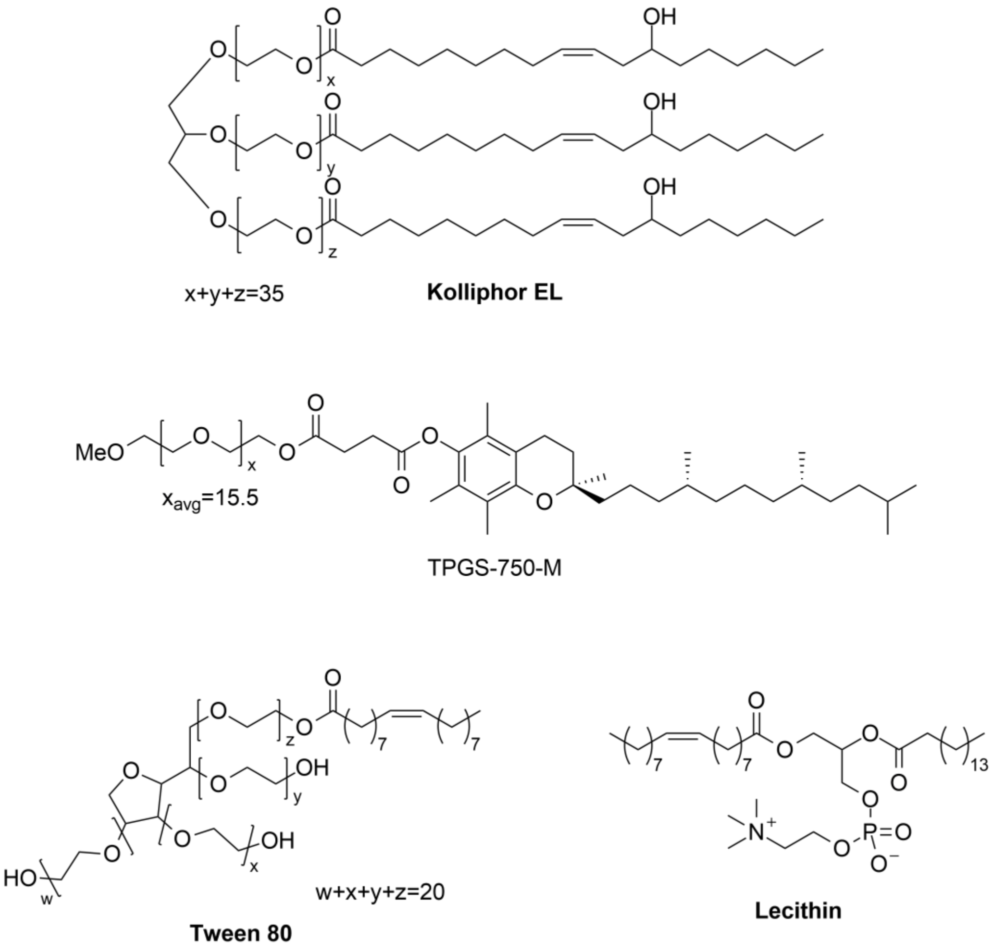

Scheme S1 Structure of the main component of surfactants selected to attempt the synthesis of PyPBTM-H

Using the same protocol, we also tried to synthesize PyPBTM directly from PyBTM. All the attempts however failed, as the protonated PyPBTM-H product was always recovered from the reaction mixture.

Protocols for the synthesis of PyPBTM-H, PyPBTM-H and PyPBTM-H

The emulsion of toluene in aqueous 2 wt% K-EL is prepared homogenizing a 2 wt% aqueous dispersion of K-EL (18 g of Kolliphor EL in 882 mL of deionized water) with 100 mL of toluene using a T 25 digital ULTRA-TURRAX® until a stable, milky dispersion is obtained. This emulsion is deoxygenated by bubbling nitrogen in the refluxing mixture for three hours before use. Triethylamine is deoxygenated by freeze-pump-thaw degassing before use.

Synthesis of PyPBTM-H

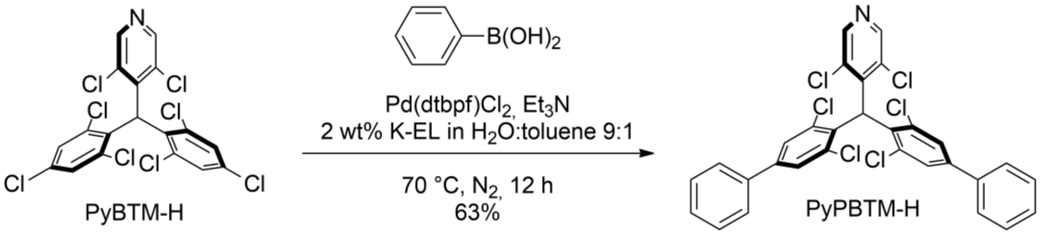

In a 25 mL roundbottom flask, PyBTM-H (521 mg, 1,00 mmol), phenylboronic acid (366 mg, 3.00 mmol) and Pd(dtbpf)Cl_2 (52.3 mg, 0.0800 mmol) are put under nitrogen atmosphere. 3.5 mL of degassed K-EL 2 wt%:toluene (9:1 v/v) emulsion are added in the flask, and the inhomogeneous mixture is heated up to 70 °C. Degassed triethylamine (0.83 mL, 6.0 mmol) is finally added. The reaction is stirred for 24 hours, then poured in 50 mL of dichloromethane and filtered on a pad of celite. The solvent is evaporated, and the crude is taken up with methanol. An off-white powder precipitates, which is filtered off, and corresponds to the pure product. 380 mg, 63% yield.
Calcd: C, 59.64; H, 2.84; N, 2.32. Found: C, 59.31; H, 2.49; N, 2.39.
^{1}H NMR (400 MHz, CD_2Cl_2): δ 8.55 (s, 1H), 8.42 (s, 1H), 7.71 (d, J=2.0 Hz, 1H), 7.69 (d, J=2.0 Hz, 1H), 7.67-7.64 (m, 4H), 7.57 (d, J=2.0 Hz, 1H), 7.55 (d, J=2.0 Hz, 1H), 7.54-7.49 (m, 4H), 7.47-7.43 (m, 2H), 6.93 (s, 1H).
^{13}C NMR (100 MHz, CD_2Cl_2): δ 149.21, 147.47, 144.48, 142.34, 142.28, 137.75, 137.60, 137.54, 137.13, 137.07, 134.62, 133.02, 132.72, 129.05, 128.65, 128.59, 128.33, 126.89, 126.81, 126.73, 50.16.

Synthesis of PyNBTM-H

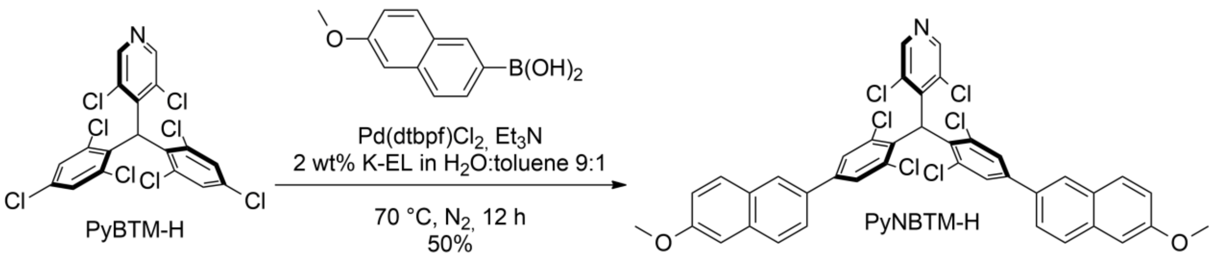

In a 25 mL roundbottom flask, PyBTM-H (521 mg, 1,00 mmol), 6-methoxy-2-naphthaleneboronic acid (606 mg, 3.00 mmol) and Pd(dtbpf)Cl_2 (52.3 mg, 0.0800 mmol) are put under nitrogen atmosphere. 3.5 mL of degassed K-EL 2 wt%:toluene (9:1 v/v) emulsion are added in the flask, and the inhomogeneous mixture is heated up to 70 °C. Degassed triethylamine (0.83 mL, 6.0 mmol) is finally added. The reaction is stirred for 12 hours, then poured in 20 mL of dichloromethane and filtered on a pad of silica. The solvent is evaporated, and the crude is further purified by column chromatography (eluent: CH_2Cl_2/heptane 1:1) to afford 380 mg of pure product (50% yield) as a white powder.
Calcd: C, 62.86; H, 3.30; N, 1.83. Found: C, 62.61; H, 2.95; N, 2.08.
^{1}H NMR (400 MHz, CD_2Cl_2): δ 8.56 (s, 1H), 8.43 (s, 1H), 8.07 (s, 2H), 7.89 (d, J=8.6 Hz, 2H), 7.86 (d, J=9.9 Hz, 2H), 7.82 (dd, J=6.8, 2.0 Hz, 2H), 7.75 (dd, J=8.6, 2.0 Hz, 2H), 7.68 (dd, J=9.6, 2.0 Hz, 2H), 7.24-7.22 (m, 4H), 6.96 (s, 1H), 3.98 (s, 6H).
^{13}C NMR (100 MHz, CD_2Cl_2): δ 158.43, 149.45, 147.71, 144.30, 142.30, 142.24, 137.82, 137.65, 137.21, 137.14, 134.56, 134.51, 133.60, 132.81, 132.53, 132.51, 129.82, 128.95, 128.59, 128.27, 127.63, 126.84, 126.67, 125.86, 124.95, 119.52, 105.57, 55.35, 50.17.

Synthesis of PyPhBTM-H

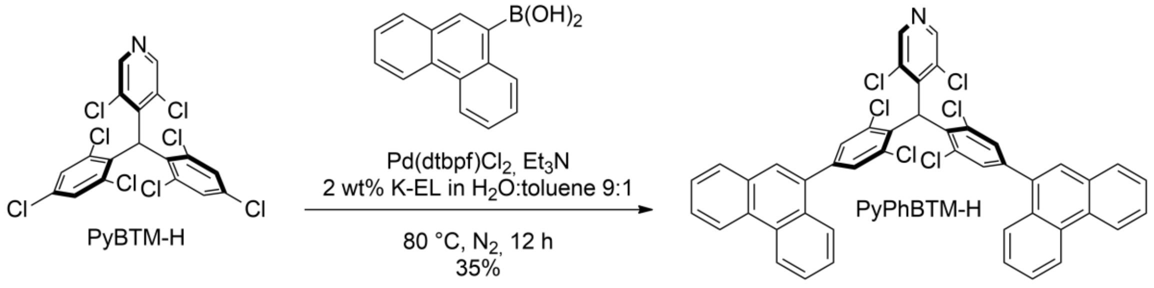

In a 25 mL roundbottom flask, PyBTM-H (521 mg, 1,00 mmol), 9-phenanthreneboronic acid (666 mg, 3.00 mmol) and Pd(dtbpf)Cl_2 (52.3 mg, 0.0800 mmol) are put under nitrogen atmosphere. 3.5 mL of degassed K-EL 2 wt%:toluene (9:1 v/v) emulsion are added in the flask, and the inhomogeneous mixture is heated up to 80 °C. Degassed triethylamine (0.83 mL, 6.0 mmol) is finally added. The reaction is stirred for 12 hours, then poured in 20 mL of dichloromethane and filtered on a pad of silica. The solvent is evaporated, and the crude is further purified by column chromatography (eluent: heptane/Et_2O/AcOEt 7:2:1) to afford 280 mg of pure product (35% yield) a white powder.

Calcd: C, 68.68; H, 3.13; N, 1.74. Found: C, 68.37; H, 2.89; N, 1.97.

^{1}H NMR (400 MHz, CD_2Cl_2): δ 8.80 (d, J=8.3 Hz, 2H), 8.73 (d, J=8.3 Hz, 2H), 8.60 (s, 1H), 8.49 (s, 1H), 7.93-7.90 (m, 4H), 7.76-7.60 (m, 12H), 7.55 (d, J=1.8 Hz, 1H), 7.49 (d, J=1.8 Hz, 1H), 7.10 (s, 1H).

^{13}C NMR (100 MHz, CD_2Cl_2): δ 149.56, 147.80, 144.31, 142.34, 142.28, 137.44, 137.30, 136.76, 136.70, 135.35, 134.63, 133.73, 133.48, 133.20, 131.85, 131.49, 131.20, 130.63, 130.22, 130.18, 130.09, 129.94, 128.83, 128.04, 127.25, 127.14, 126.99, 126.89, 126.15, 123.11, 122.57, 50.38.

Protocols for the synthesis of PyPBTM, PyPBTM and PyPBTM

All the reactions are performed adapting literature conditions used to synthesize PyBTM from PyBTM-H.[1]

Synthesis of PyPBTM

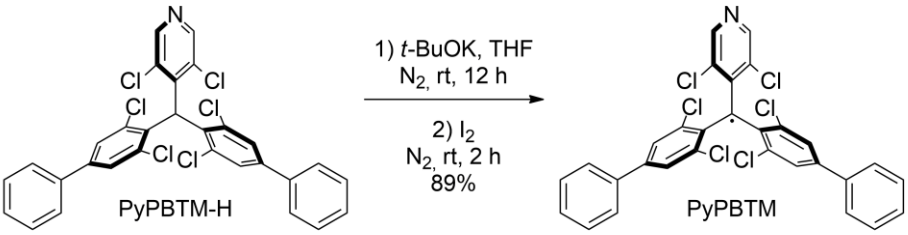

In a 100 mL roundbottom flask, PyPBTM-H (460 mg, 0.761 mmol) is put under N_2 atmosphere and dissolved in anhydrous THF (30 mL), then *t*-BuOK (300 mg, 2.67 mmol) is added portionwise. The solution is allowed to stir overnight at room temperature in the dark. In another flask, iodine (1.121 g, 4.417 mmol) is dissolved in THF (10 mL), and the solution is added in the flask containing the carbanion. The reaction is stirred at room temperature for 2 more hours. Solvent is evaporated under reduced pressure, and the residue is eluted through a pad of silica (eluent: heptane/DCM 1:2) to afford 410 mg of product in the form of a shiny, black powder (0.680 mmol, 89% yield). Mp 234-235 °C.

HRMS (negative ion mode ESI-TOF) m/z: $[M]^-$ Calcd for $C_{30}H_{16}NCl_6$ 599.9419; Found 599.9417.

Elem. Anal. Calcd for $C_{30}H_{16}NCl_6$: C, 59.74; H, 2.67; N, 2.32. Found: C, 59.41; H, 2.39; N, 2.45.

Synthesis of PyNBTM

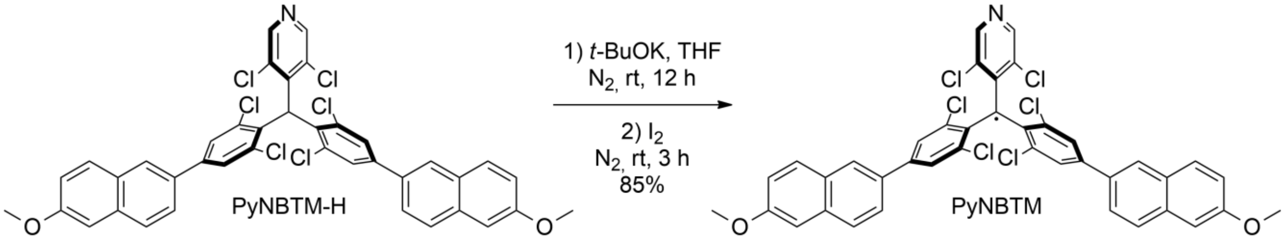

In a 50 mL roundbottom flask, PyNBTM-H (240 mg, 0.314 mmol) is put under N_2 atmosphere and dissolved in anhydrous THF (15 mL), then *t*-BuOK (126 mg, 1.12 mmol) is added portionwise. The solution is allowed to stir overnight at room temperature in the dark. In another flask, iodine (472 mg, 1.86 mmol) is dissolved in THF (5 mL), and the solution is added in the flask containing the carbanion. The reaction is stirred at room temperature for 3 more hours. Solvent is evaporated under reduced pressure, and the residue is eluted through a pad of silica (eluent: heptane/DCM 1:2) to afford 204 mg of product in the form of a shiny, dark green powder (0.267 mmol, 85% yield). Mp 234-236 °C.

HRMS (negative ion mode ESI-TOF) m/z: $[M]^-$ Calcd for $C_{40}H_{24}NO_2Cl_6$ 759.9944; Found 759.9925.

Calcd for $C_{40}H_{24}NO_2Cl_6$: C, 62.94; H, 3.17; N, 1.83. Found: C, 62.72; H, 2.89; N, 1.99.

Synthesis of PyPhBTM

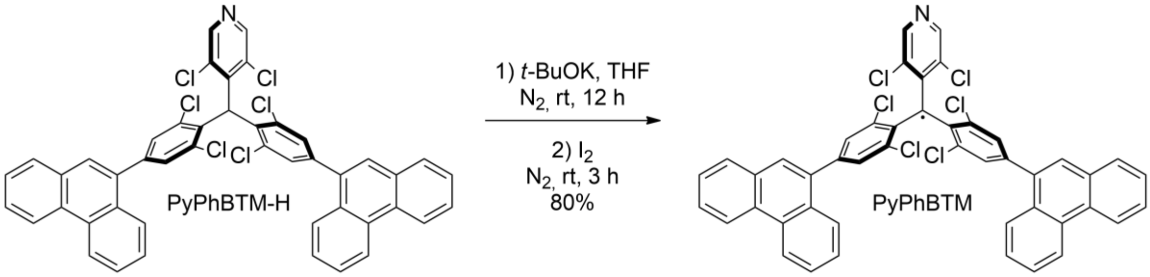

PyPhBTM-H (100 mg, 0.124 mmol) is put under N_2 atmosphere and dissolved in anhydrous THF (8.0 mL), then *t*-BuOK (49 mg, 0.44 mmol) is added portionwise. The solution is allowed to stir overnight at room temperature in the dark. In another flask, iodine (183 mg, 0.721 mmol) is dissolved in THF (3.0 mL), and the solution is added in the flask containing the carbanion. The reaction is stirred at room temperature for 3 more hours. Solvent is evaporated under reduced pressure, and the residue is eluted through a pad of silica (eluent: heptane/DCM 1:2) to afford 80 mg of product in the form of a shiny, black powder (0.0100 mmol, 80% yield). Mp 235-236 °C.
HRMS (negative ion mode ESI-TOF) m/z: $[M]^-$ Calcd for $C_{46}H_{24}NCl_6$ 800.0045; Found 800.0058.
Calcd for $C_{46}H_{24}NCl_6$: C, 68.77; H, 3.01; N, 1.74. Found: C, 68.41; H, 2.94; N, 1.88.

S2. Optical characterization in solution

Instrumentation

Absorption coefficients were determined using a JASCO V-770 spectrometer.

Photoluminescence (PL) spectra and photostability under 370 nm light were recorded with a JASCO FP-8600KS spectrofluorometer.

Temperature dependence of PL spectra were measured with a temperature controller UNISOKU CoolSpeK USP-203.

Absolute luminescence quantum yields (Φ_f) were measured using a Hamamatsu Photonics Quantaurus-QY C11347 by mean of an integrating sphere. PyPBTM, PyNBTM and PyPhBTM were excited at 400 nm, 440 nm, and 420 nm respectively. The quantum yield was calculated as (Intensity of fluorescence)/(Intensity of absorbed incident light). The dominating error comes with the accuracy of sample replacement and the accurate replacement of the upper half of the sphere after changing the sample. These two factors particularly affect the accurate determination of the “absorbed area”. With a good and careful routine we can estimate an absolute error of ±2%.

Fluorescence lifetimes (τ_f) were measured using a Hamamatsu Photonics Quantaurus-Tau C11367, in all the cases using an excitation wavelength of 405 nm.

Room temperature characterization in cyclohexane

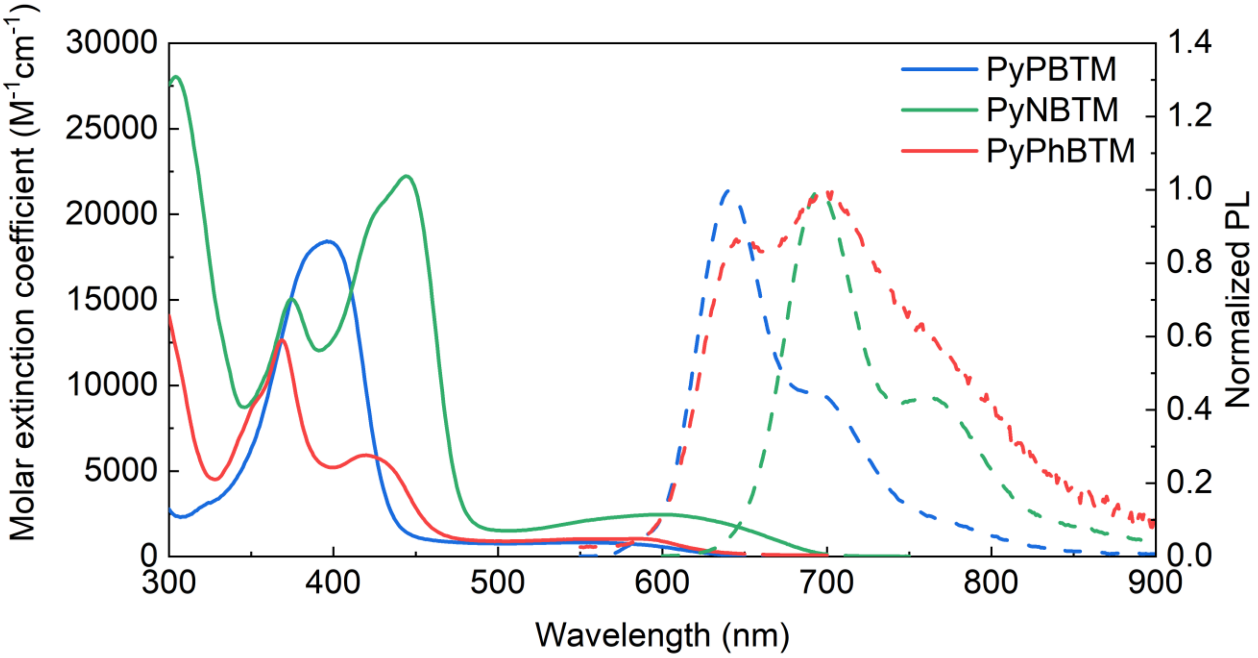

Figure S1 UV-Vis absorption (continuous line) and normalized emission (dashed line) spectra of luminescent radicals PyPBTM, PyNBTM and PyPhBTM in cyclohexane. PL spectra were recorded exciting PyPBTM, PyNBTM and PyPhBTM at 420 nm, 450 nm, and 500 nm respectively.

Temperature-dependent characterization in EPA (diethyl ether:isopentane:ethanol 5:5:2 v/v)

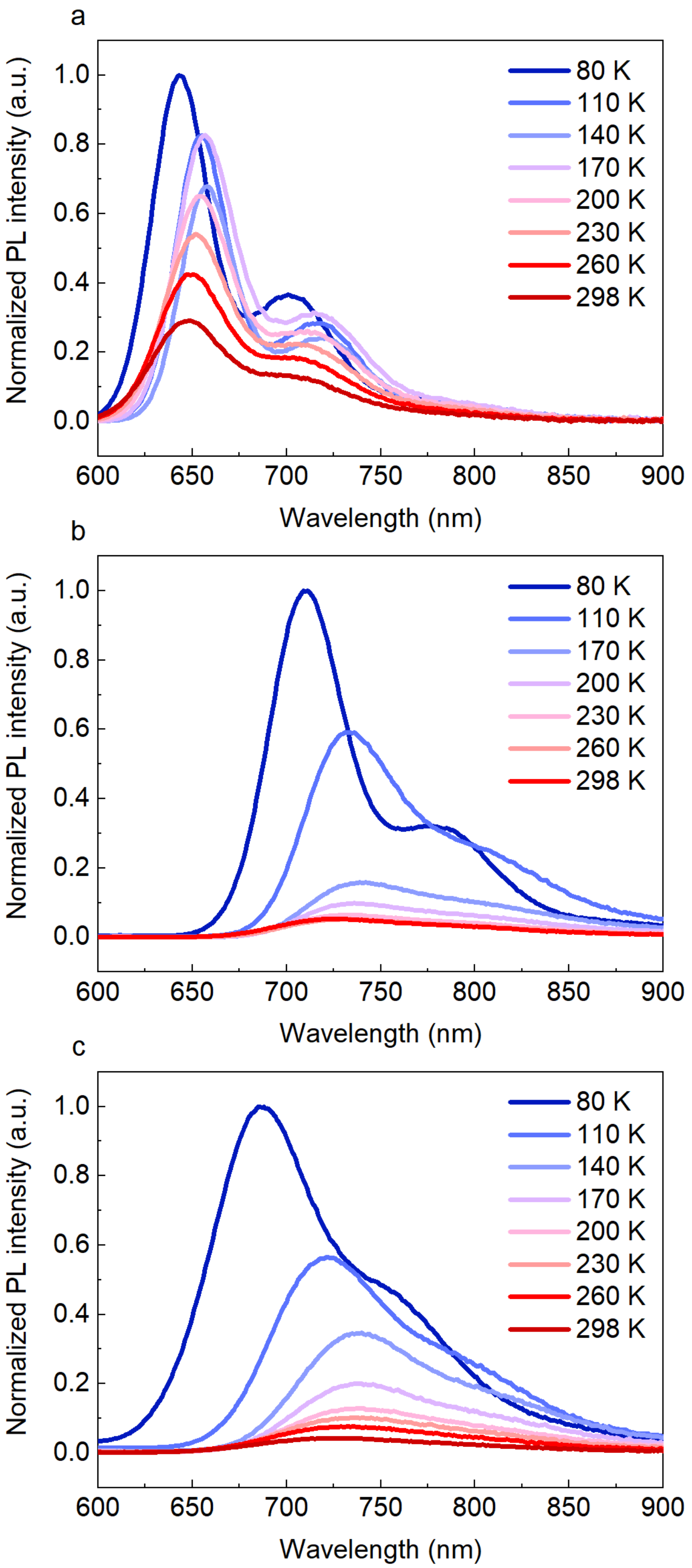

Figure S2 Temperature dependence of PL spectra of a) PyPBTM, b) PyNBTM and c) PyPhBTM in EPA solution. PL intensities are normalized with respect to the highest observed intensity, in all the cases obtained @80 K.

Lifetime of all derivatives in various media

PyPBTM

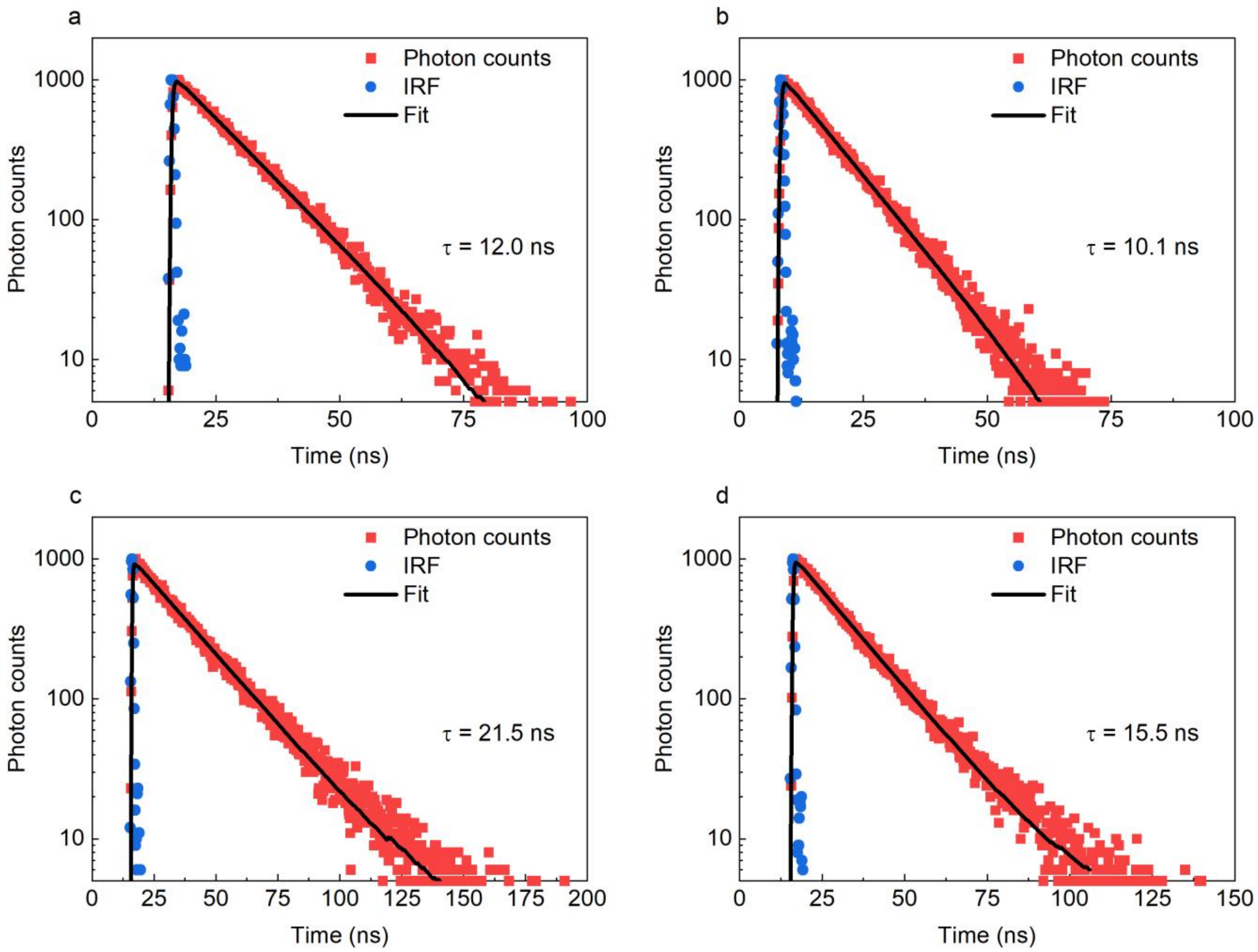

Figure S3 Red squares represent the PL decay of the excited state of PyPBTM in a) chloroform solution (at room temperature), b) cyclohexane solution (at room temperature), c) EPA (@77 K) and d) PMMA matrix (at room temperature). Blue circles show the instrument response factor (IRF). Lifetime of the excited state in the various media is determined through the fitting of the decay (black line).

PyNBTM

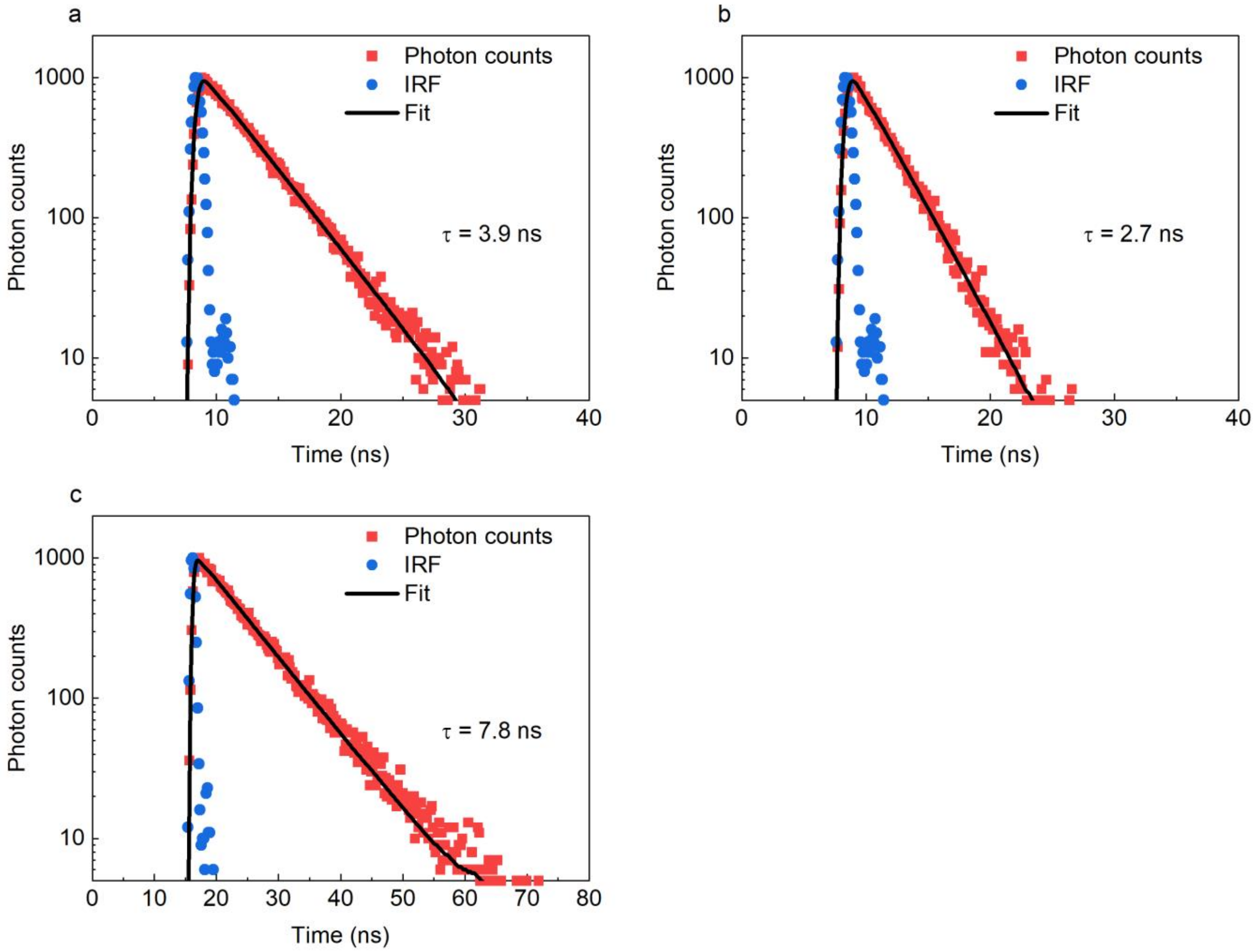

Figure S4 Red squares represent the PL decay of PyNBTM in a) chloroform solution (at room temperature), b) cyclohexane solution (at room temperature), and c) EPA (@77 K). Blue circles show the instrument response factor (IRF). Lifetime of the excited state in the various media is determined through the fitting of the decay (black line).

PyPhBTM

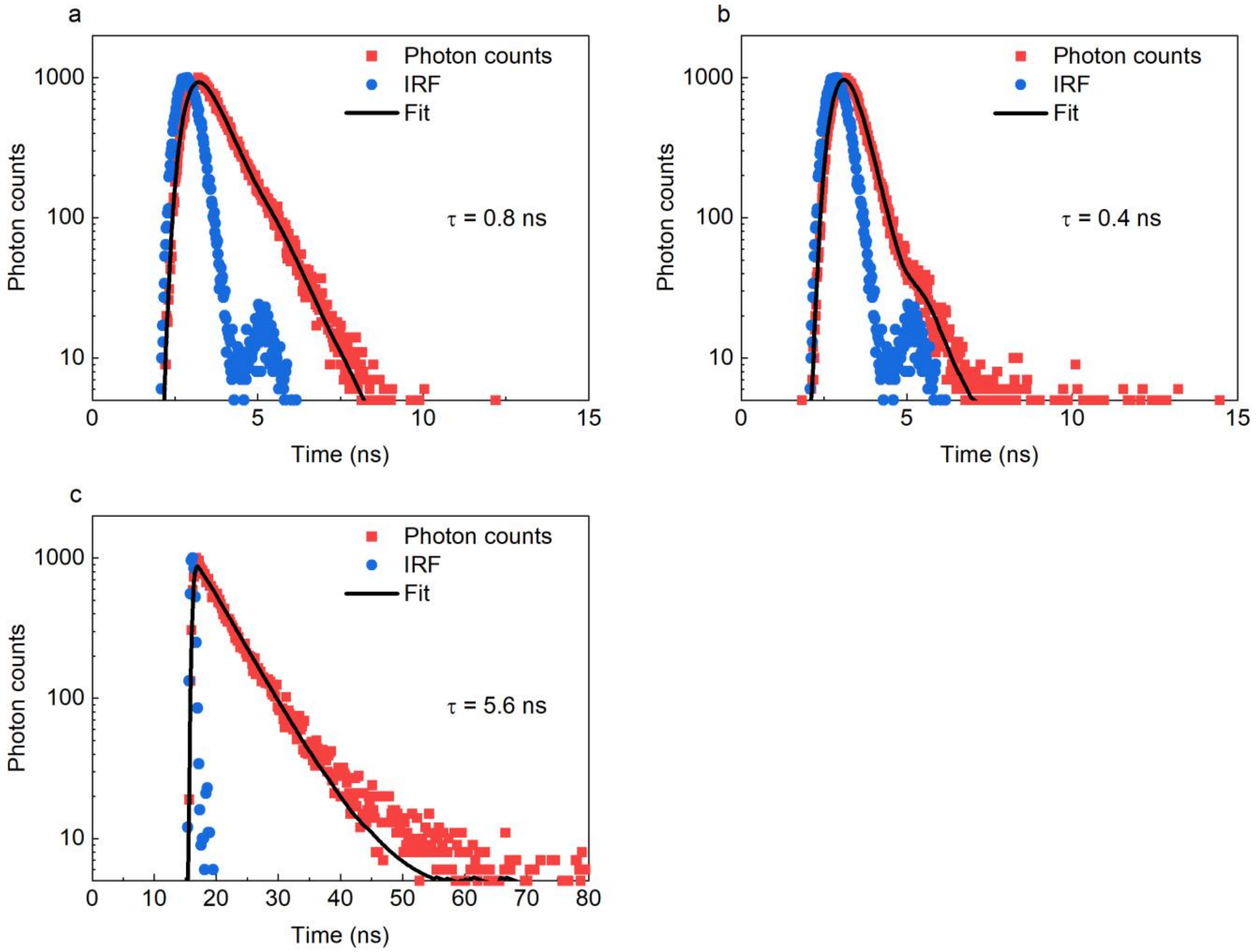

Figure S5 Red squares represent the PL decay of PyPhBTM in a) chloroform solution (at room temperature), b) cyclohexane solution (at room temperature), and c) EPA (@77 K). Blue circles show the instrument response factor (IRF). Lifetime of the excited state in the various media is determined through the fitting of the decay (black line).

S3. Electrical characterization in solution

Instrumentation and methods

Electrochemical measurements were recorded at 50 mV s^{-1} with an EG&G Princeton Applied 2273 potentiostat/galvanostat within an argon filled glovebox. The working electrode was a 3 mm glassy carbon electrode; a platinum mesh served as auxiliary electrode, and the reference electrode was an Ag^+/Ag electrode (a silver wire immersed in 0.1 M Bu_4NClO_4/0.01 M $AgCl_2$/DCM). Ferrocene was used as an internal standard for calibrating potentials.

Cyclovoltammetries

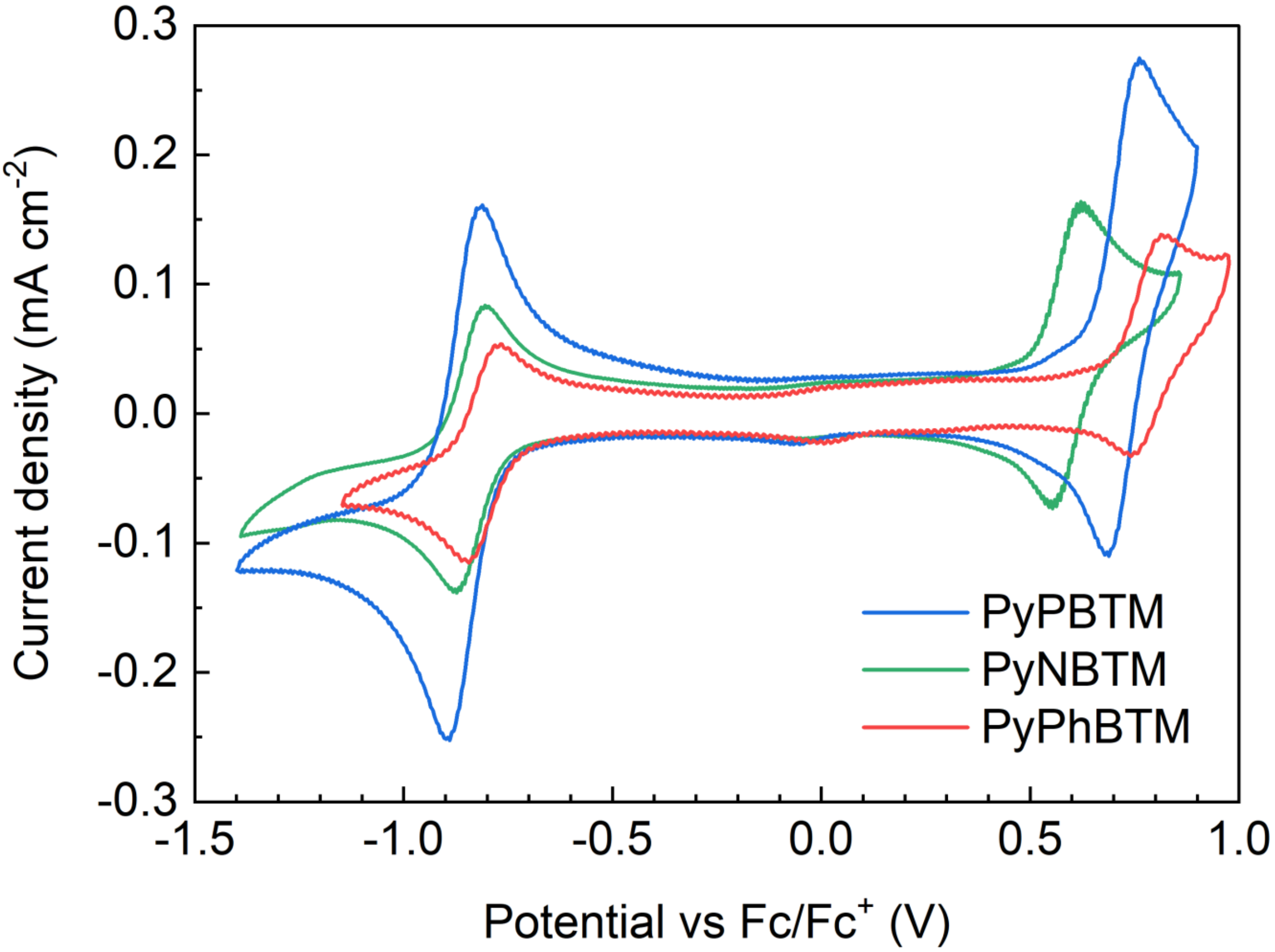

Differential pulsed voltammetries

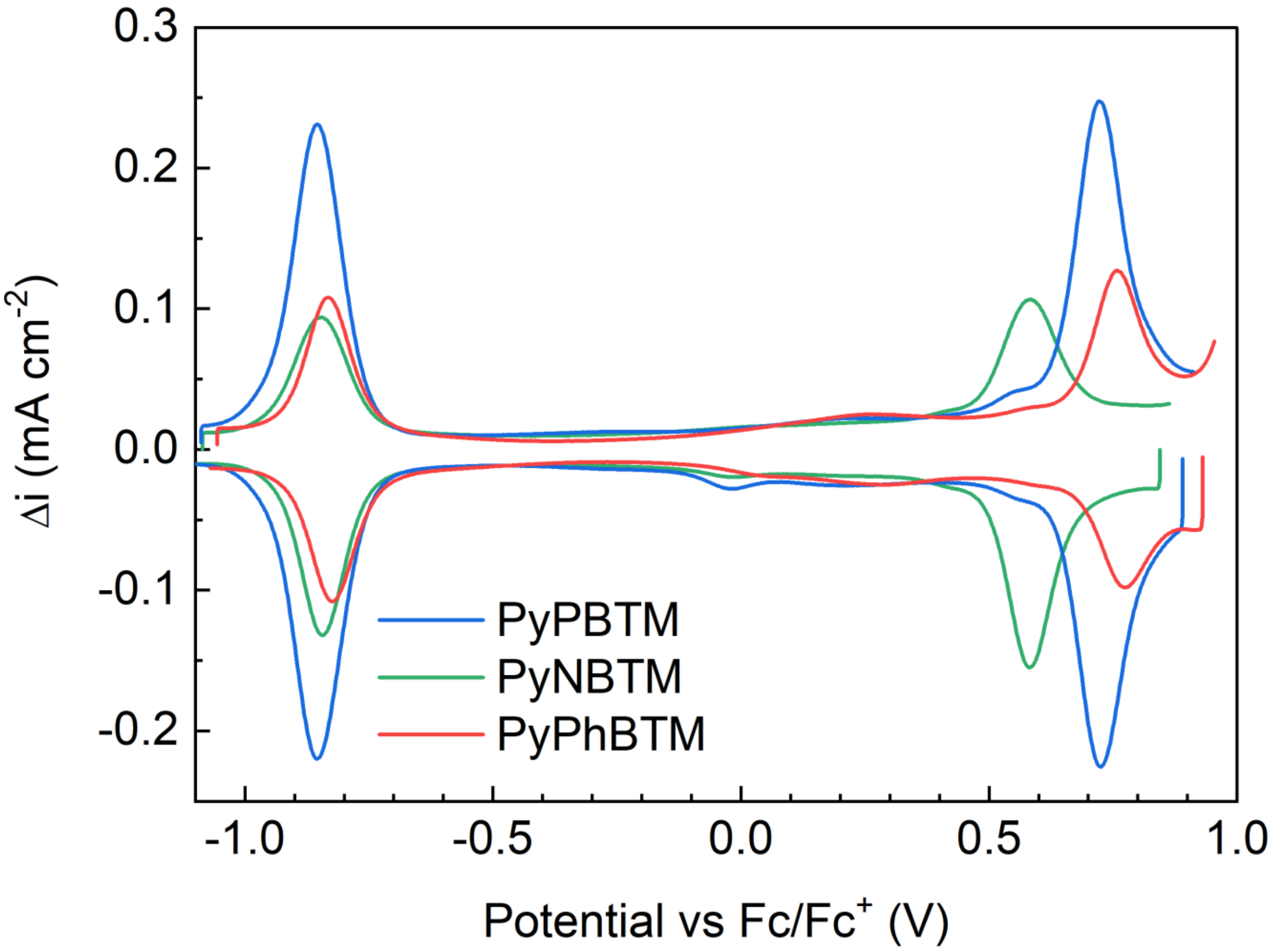

Oxidation and reduction potentials vs Fc$^+$/Fc; HOMO and LUMO levels of all radicals

Fc$^+$/Fc at 0.7 V vs. NHE (Sawyer); NHE at 4.6 V vs vacuum (Bockris), ergo Fc$^+$/Fc at 5.3 V vs vacuum

	Ox vs. Fc$^+$/Fc (V)	**Red vs. Fc$^+$/Fc (V)**	**HOMO (eV)**	**LUMO (eV)**
PyPBTM	+0.730 ± 0.005	-0.840 ± 0.010	-6.03 ± 0.1	-4.46 ± 0.1
PyNBTM	+0.570 ± 0.005	-0.860 ± 0.005	-5.87 ± 0.1	-4.44 ± 0.1
PyPhBTM	+0.760 ± 0.010	-0.840 ± 0.010	-6.06 ± 0.1	-4.46 ± 0.1

S4. Details on theoretical calculations

Methods

Atomistic simulations of PyBTM and of its PyPBTM, PyPhBTM and PyNBTM derivatives have been carried out by following a multilevel protocol. First, stable conformers of the molecules have been found by using a semiempirical tight-binding approach. The GFN2-xTB Hamiltonian[2] has been used as "engine" for the search of minimum energy configurations through an automated conformer-rotamer ensemble sampling tool (CREST).[3,4] Then, electronic and optical properties of the molecules have been investigated using (time-dependent) density functional theory simulations, performed in a GTO framework by using the ORCA suite of programs.[5,6] In detail, the Kohn-Sham orbitals have been expanded on an all-electron def2-TZVPP Gaussian type basis set.[7,8] The corresponding def2/J basis has been also used as an auxiliary basis set for Coulomb fitting in a resolution-of-identity/chain-of-spheres (RIJCOSX) framework. Molecular geometries have been fully optimized and their properties investigated by using the B3LYP functional,[9] with the addition of the pairwise D3 correction for the calculation of dispersion forces.[10] Absorption spectra have been calculated using time-dependent density functional theory at the same B3LYP@def2-TZVPP level of theory. A large basis of 600 vectors connecting occupied and unoccupied Kohn-Sham orbitals has been used to build the Davidson expansion space for the calculations of the first 30 electronic transitions of all the molecules. The absorption and emission vibronic spectra have been calculated by using the independent mode displaced harmonic oscillator (IMDHO) model, as implemented in the ORCA advanced spectral analysis (ASA) module.

Frontier orbitals and theoretical optoelectronic properties of all derivatives

Table S1 Optoelectronic properties of PyBTM and of its PyPBTM, PyPhBTM and PyNBTM derivatives, calculated at the B3LYP@def2-TZVPP level of theory. Upper part: unrestricted Kohn-Sham frontier orbitals. Lower part: main absorption and emission lines calculated using TDDFT. In the case of absorption, two contributions are reported, labelled A and B in Figure 3 and corresponding to the onset of absorption (D0→D1) and to the strongest absorption (UV-Vis λ_{max})

B3LYP@ def2-TZVPP (eV)	**PyBTM**		**PyPBTM**		**PyPhBTM**		**PyNBTM**	
	↑ (α)	↓ (β)	↑ (α)	↓ (β)	↑ (α)	↓ (β)	↑ (α)	↓ (β)
LUMO+1	-1.54	-1.44	-1.75	-1.68	-1.71	-1.66	-1.71	-1.63
LUMO	-1.75	-1.64	-1.78	-1.69	-1.72	-1.68	-1.72	-1.67
SUMO	-	-3.61	-	-3.54	-	-3.50	-	-3.45
SOMO	-5.87	-	-5.66	-	-5.61	-	-5.41	-
HOMO	-7.07	-7.04	-6.67	-6.64	-6.04	-6.04	-5.84	-5.84

Optical properties (nm)

D0→D1 **β-HOMO→β -SUMO character**	505 87%	540 85%	600 89%	637 88%
UV-Vis λ_{max}	376[a]	409[b]	394[c]	407[d]
Emission maximum	579	620	663	666

[a] The strong absorption band peaked at 376 nm is a convolution of two electronic transitions at 378 nm (58% α-SOMO→α-LUMO character) and 375 nm (67% α-SOMO→α-LUMO+1 character).

[b] The strong absorption band peaked at 409 nm is a convolution of three electronic transitions at 415 nm (42% α-SOMO→α-LUMO character), 405 nm (complex transition mainly involving β orbitals) and 398 nm (37% α-SOMO→α-LUMO+1 character).

[c] The strong absorption band peaked at 394 nm is a convolution of two electronic transitions at 394 nm (40% α-SOMO→α-LUMO character) and 393 nm (42% α-SOMO→α-LUMO+1 character).

[d] The strong absorption band peaked at 407 nm is a convolution of two distinct groups of electronic transitions; a first one at 472 nm (39% α-SOMO→α-LUMO character), and a group of four at 423 nm (complex transition mainly involving several β orbitals), 411 nm (21% α-SOMO→α-LUMO character), 399 nm (35% α-SOMO→α-LUMO+1 character) and 396 nm (complex transition mainly involving several β orbitals).

S5. Spectral overlap of PyPBTM with respect to commercial luminophores

A quantitative comparison of the spectral overlap between **PyPBTM** and reference commercial luminescent dyes (**Lumogen F Violet 570** and **Lumogen F Red 305**) is offered.
The absorbance and normalized emission spectra of all considered luminophores are reported in Figure S6.

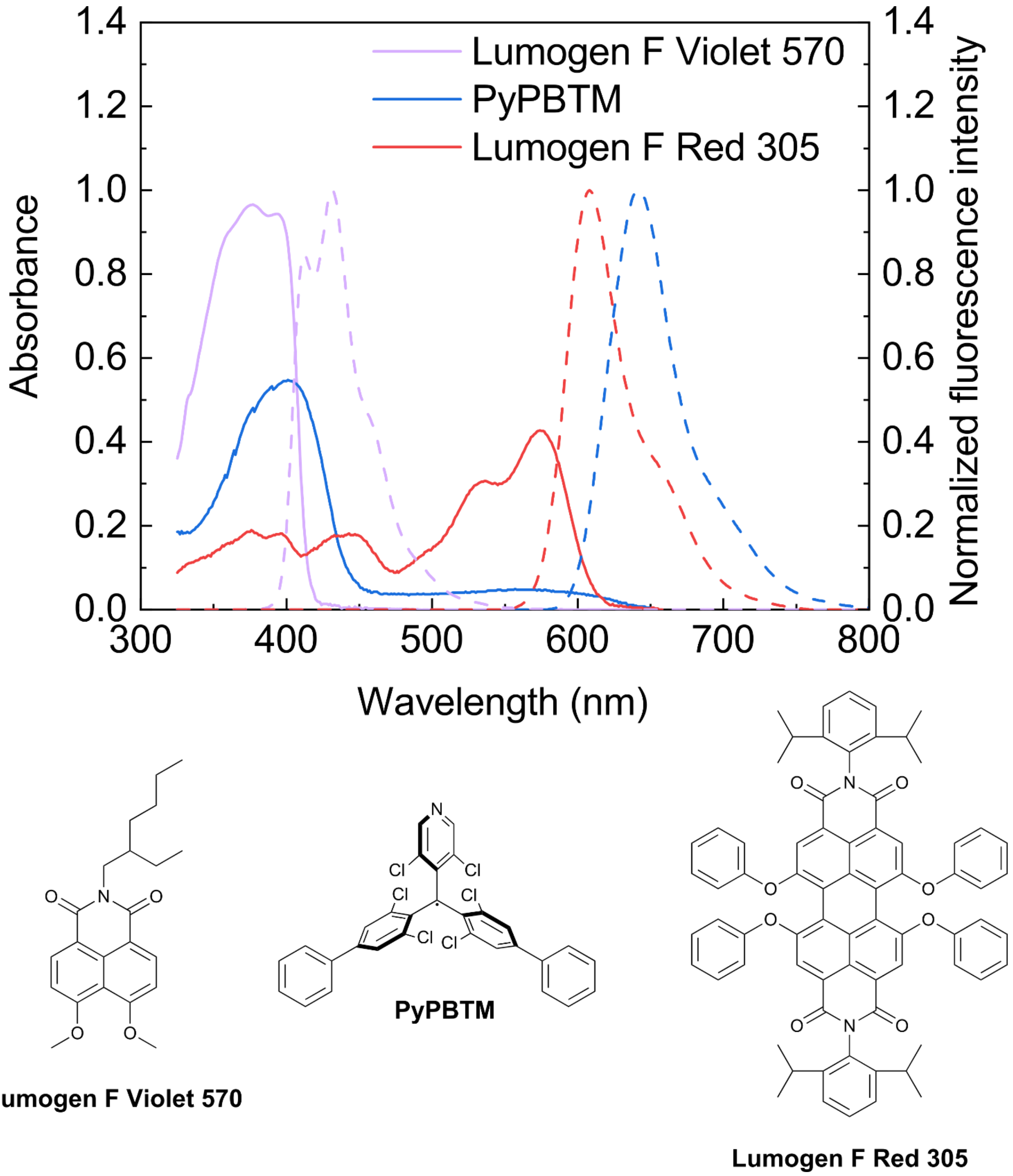

Lumogen F Violet 570

PyPBTM

Lumogen F Red 305

Figure S6 Absorption spectra, normalized fluorescence spectra, and molecular structures of Lumogen F Violet 570, Lumogen F Red 305 and PyPBTM

The overlap coefficient was evaluated according to two different definitions reported in the literature.

1. **Radiative overlap (RO)** defined as the fraction of the emitted light that can be re-absorbed by the dye itself:

$$RO = \frac{\int Em(\lambda)[1 - T(\lambda)]d\lambda}{\int Em(\lambda)d\lambda} \cdot 100$$

where $Em(\lambda)$ is the emission spectrum, $[1 - T(\lambda)]$ the fraction of absorbed light and $T(\lambda)$ is the transmission spectrum obtained through UV-Vis absorption measurements.

RO should be as small as possible to ensure minimum reabsorption (RO → 0 for an emitter with perfectly non-overlapping absorption and emission spectra).[11]

2. Overlap coefficient defined by the **weighted quality factor (<Q>)**, given by the ratio between the absorption coefficient at the wavelength of maximum absorbance ($\alpha_1(\lambda_{abs\,max})$) and the value of absorption coefficient ($< \alpha_2 >$) averaged across the emission region:

$$< Q > = \frac{\alpha_1(\lambda_{abs\,max})}{< \alpha_2 >}$$

with:

$$< \alpha_2 > = \frac{\int Em(\lambda)\, \alpha(\lambda)d\lambda}{\int Em(\lambda)d\lambda}$$

and α(λ) being the absorption coefficient in the emission spectral region.

<Q> should be as large as possible to ensure minimum reabsorption (Q → ∞ for an emitter with perfectly non-overlapping absorption and emission spectra).[12]

Results

1. Radiative overlap (RO)

Radiative overlap (RO)		
Lumogen F Violet 570	**PyPBTM**	**Lumogen F Red 305**
0.095	0.008	0.081
9.5%	0.8%	8.1%

2. Weighted quality factor (<Q>)

Weighted quality factor (<Q>)		
Lumogen F Violet 570	**PyPBTM**	**Lumogen F Red 305**
20	92	6

PyPBTM luminophore shows remarkably better performance (lower spectral overlap) according to both figures of merit. In particular, the RO value of **PyPBTM** is more than 10 times lower than that of commercial dyes. Also, the extremely high <Q> value of **PyPBTM** luminophore demonstrates that **PyPBTM** is a nearly perfect emitter with negligible contribution of reabsorption losses.

S6. Materials, methods and characterizations in LSC devices

Materials

Chloroform ($CHCl_3$) was from Sigma-Aldrich and used as received. Poly(methyl methacrylate)–PMMA (ALTUGLAS® BS 550) was purchased from Arkema and used as polymeric carrier in luminescent coatings. Lumiflon LF-910LM was purchased from Asahi Glass Company Ltd. Vestanat T1890/100 was provided by Evonik.

Fabrication of PyPBTM-based LSC devices

Preparation of PyPBTM/PMMA LSCs

LSCs were fabricated in thin-film configuration starting from $CHCl_3$ solutions of PMMA (15 wt%) with various concentrations of **PyPBTM** 3 (0.1-7 wt% with respect to dry polymer). **PyPBTM**/PMMA films were obtained by spin coating (1200 rpm for 60 s) onto 5.0 × 5.0 × 0.6 cm^3 N-BK7 glass slabs using a Laurell WS-400BZ-6NPP/LITE instrument.

Preparation of PyPBTM/F-PU LSCs

For the preparation of crosslinking system (from now on referred to as F-PU), a 25 wt% $CHCl_3$ solution of Lumiflon LF910-LM (100 mg KOH/g polymer) and Vestanat T1890/100 was prepared under magnetic stirring (NCO/OH = 0.97), followed by the addition of **PyPBTM** (3 wt%). Right before the spin-coating deposition process, a catalyst solution (di-n-butyltin dilaurate in chloroform, 0.2 wt%) was added to the system. The obtained solution was then spin-cast onto the glass substrates in air (1000 rpm, 40 s) and allowed to crosslink in an oven at 150 °C for 20 min.

Optical characterization

UV–Vis absorption spectra were recorded on a Thermo Scientific Evolution 600 UV–Vis spectrophotometer using wavelength scan with a resolution of 1 nm at a scan speed of 120 nm/min and a slit width of 2 nm. Fluorescence spectroscopy analyses were performed both in front-face emission configurations and edge-emission configuration on a Jasco FP-6600 spectrofluorometer.

Internal and external photon efficiency (ηint, ηext) measurements were performed by illuminating the top face of the LSC using an Abet Technologies Sun 2000 solar simulator with AM1.5G filter (irradiance of 1000 ± 10 W m-2) and by collecting the edge emission of the LSC devices with a spectroradiometer (International Light Technologies ILT950) equipped with a cosine corrector positioned at the center of the edge, while the other edges were covered with black tape. The edge-emission spectra of the LSCs were recorded using Spectralight software. The above cited tests were repeated for at least three devices. Reabsorption losses were evaluated using a 20.0 × 5.0 × 0.6 cm3- sized LSC device fabricated with a N-BK7 glass substrate. An Abet Technologies Sun 2000 solar simulator equipped with AM1.5G filter (irradiance of 1000 ± 10 W m-2) was used in conjunction with the spectroradiometer set-up to collect single-edge output optical power. The irradiation of the top surface was confined to a single circular spot (diameter = 3 cm) by means of a holed black mask, which was systematically moved to vary the optical path length.

Photostability tests were carried out under UV-A light in non-inert (air) atmosphere using a UV polymerization apparatus (Helios Quartz, POLIMER 400W) equipped with a high-power high-pressure mercury UV-A lamp (Zs type, Helios Quartz) characterized by an emission window between 400 and 315 nm and with radiative power density equal to 350 ± 5 W m-2. The temperature was set at 45 °C and the relative humidity 25%.

Monte Carlo ray-tracing modeling

Ray-tracing simulations were performed using a graphical user interface (GUI) in MATLAB®2020b recently proposed in literature.[13] The source emission spectrum and power were set. The wavelength of the light source rays was chosen randomly according to the solar simulator spectrum (AM1.5) as measured with a spectroradiometer. The incident light (rays) was forced to the central position of the waveguide. The LSC in thin-film configuration was modeled as two plates in optical contact where the upper plate represents the polymeric coating (with refractive index fixed to 1.52 at all wavelengths) embedding the luminophore species, while the lower plate represents a high-quality glass substrate, characterized by a refractive index of 1.50 at all wavelengths and absorption coefficient equal to 10^{-3} cm^{-1}. To model the luminescent species in the coating, the absorption and emission spectra as well as the PLQY of the luminophores in PMMA were considered.

In this study, 1’000’000 input rays were employed to perform the calculations. Simulations were all conducted on a desktop computer running on a quad-core processor Intel i7-7500U at 3.5 GHz.

The modeled devices were based on the same geometry of the experimental one with thickness for the glass substrate $t_s = 0.6$ cm, thickness of the luminescent coating $t_c = 0.0005$ cm, waveguide width of 5 cm. The optical path length, *d*, between the irradiation position and the collection edge was varied by shifting the position of the source (*d* = 0.5, 2.5, 5, 7.5, 10, 15, 20, 30, 40, 50, 75, 100 cm). Integrated single-edge output optical power was calculated as the integral of the spectrum of emitted rays from the selected lateral edge of the LSC substrate.

S7. Absorbance and front-face photoluminescence spectra of PyPBTM in thin film

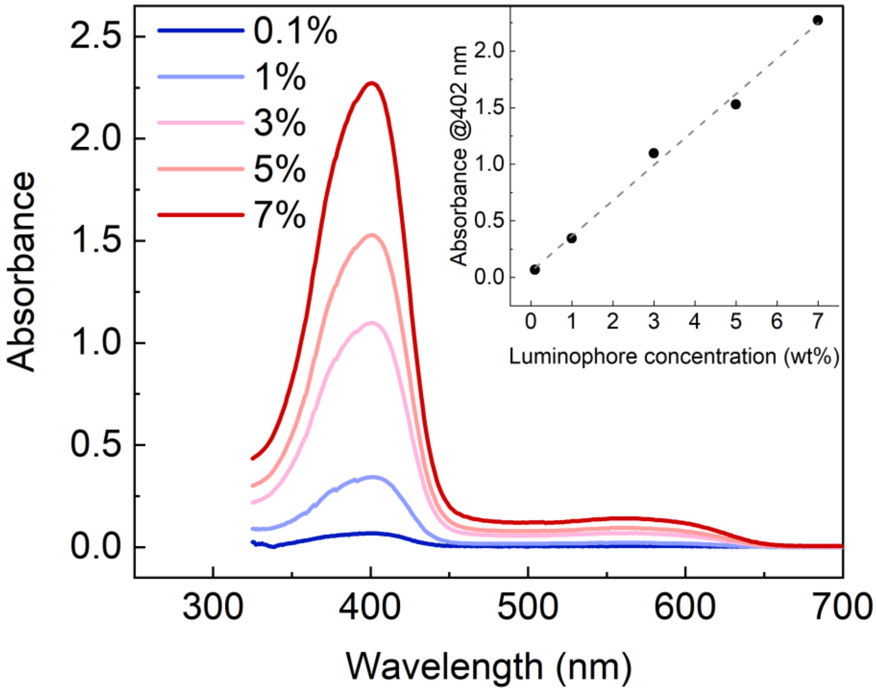

Figure S7 Absorption spectra of PyPBTM for various luminophore loading (wt%) in PMMA thin films. The inset shows the absorbance of the peak maximum (@402 nm) as a function of the luminophore concentration, highlighting the linear trend.

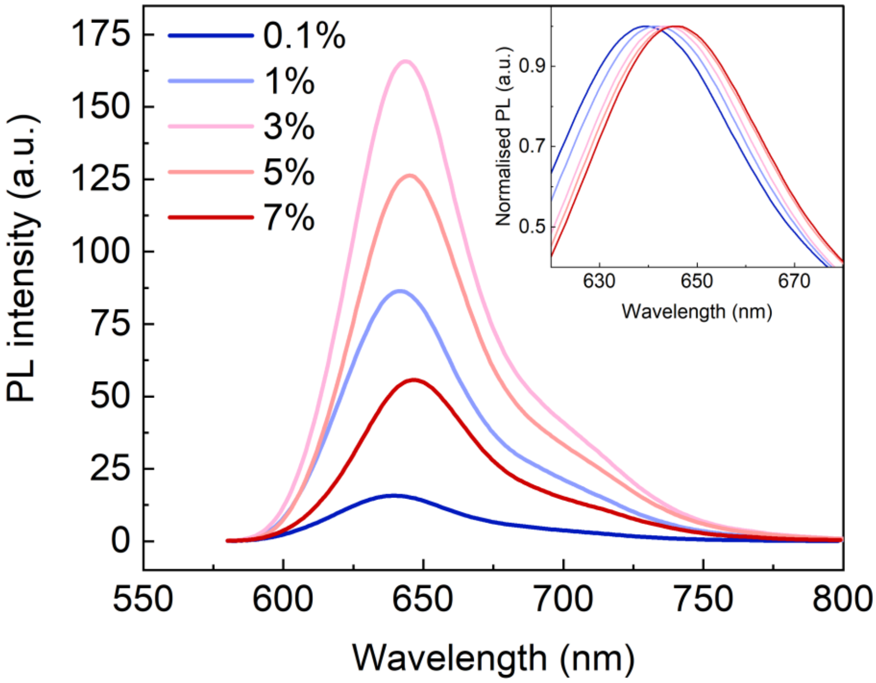

Figure S8 Emission spectra of PyPBTM as the function of the luminophore concentration (wt%) in PMMA thin films. The inset shows the normalized emission maximum, highlighting its shift at higher wavelengths with increasing luminophore loading.

S8. Optical performance of PyPBTM-based LSCs

Optical performance of PyPBTM-based LSC devices have been evaluated in terms of external and internal photon efficiency (η_{ext} and η_{int}, respectively) from the experimental data according to the equations below:

$$\eta_{ext} = \frac{N_{ph\text{-}out}}{N_{ph\text{-}in}} = \frac{\sum_{i=1}^{4} \int_{300}^{800} P_{i(out)}(\lambda)\, \frac{\lambda}{hc}\, d\lambda}{\int_{300}^{800} P_{in}(\lambda)\, \frac{\lambda}{hc}\, d\lambda} \qquad \textit{(Equation S1)}$$

$$\eta_{int} = \frac{N_{ph\text{-}out}}{N_{ph\text{-}abs}} = \frac{\sum_{i=1}^{4} \int_{300}^{800} P_{i(out)}(\lambda)\, \frac{\lambda}{hc}\, d\lambda}{\int_{300}^{800} P_{in}(\lambda)\, [1-10^{-A(\lambda)}]\, \frac{\lambda}{hc}\, d\lambda} \qquad \textit{(Equation S2)}$$

where $N_{ph\text{-}out}$ is the total number of edge-emitted photons summed over four edges (i = 1-4) of the LSC, $N_{ph\text{-}abs}$ is the total number of photons absorbed by the LSC, and $N_{ph\text{-}in}$ is the total number of photons incident on the top surface of the LSC. $P_{i(out)}(\lambda)$ is the output power spectra measured for each edge of the LSC (in $W \cdot nm^{-1}$), $P_{in}(\lambda)$ is the input power spectrum from the solar simulator incident on the top surface of the LSC (in $W \cdot nm^{-1}$), h is Planck's constant (in J·s), c is the speed of light (in $m \cdot s^{-1}$), and A(λ) is the absorption spectrum of the LSC. The integrations are performed in the 300-800 nm range of the AM1.5G solar spectrum.

S9. Photostability and encapsulation of PyPBTM-based LSCs

Photostability is a critical parameter for LSCs. PMMA was initially selected as host matrix due to its favourable optical properties (high transparency and high refractive index) and because it currently represents the material-of-choice as polymeric host matrix in state-of-the-art LSC devices. Yet, the limited photostability of PyPBTM organic radical in PMMA-based LSC devices represents an issue that can severely affect the lifetime of LSCs. As can be observed in Figure S9, under UV-A (~350 W m^{-2}) a ~55% decrease in optical power was detected after 40 min of continuous illumination, reaching a constant response after 200 min of irradiation.

With the aim of improving the stability of PyPBTM-PMMA LSC systems, the use of an alternative polymeric system that could ensure a further improvement in outdoor stability was attempted. It consists in a crosslinked polyurethane fluorinated matrix obtained from the reaction of a functional chloro-trifluoro-ethylene-co-vinyl-ether (CTFE-VE) based copolymer with an isophorone-diisocyanate (IPDI) prepolymer (F-PU in Figure S9). Clearly, a significant improvement of the photostability under UV-A light was achieved in the presence of F-PU, suggesting that the development of tailored high-durability host matrices may represent a promising strategy to preserve the emission performance of our new persistent organic radical, thus leading to LSC devices of enhanced operational lifetime.

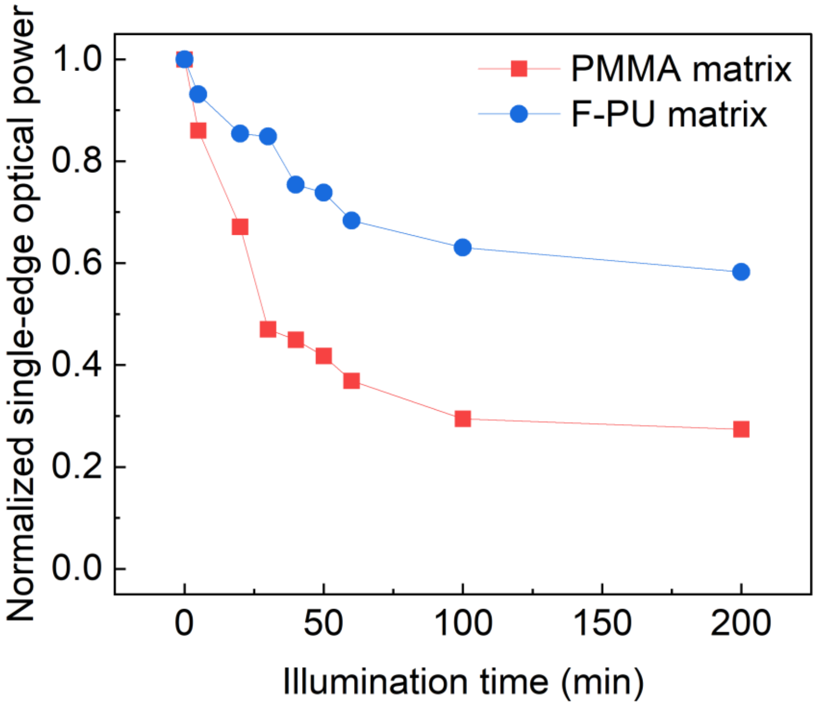

Figure S9 Photostability tests under UV-A light (350 W m^{-2}) of PyPBTM-based LSC devices. The normalized integrated single-edge optical power signals vs. illumination time are reported.

S10. NMR spectra of all derivatives

PyBTM-H, ^{1}H NMR in CDCl$_3$

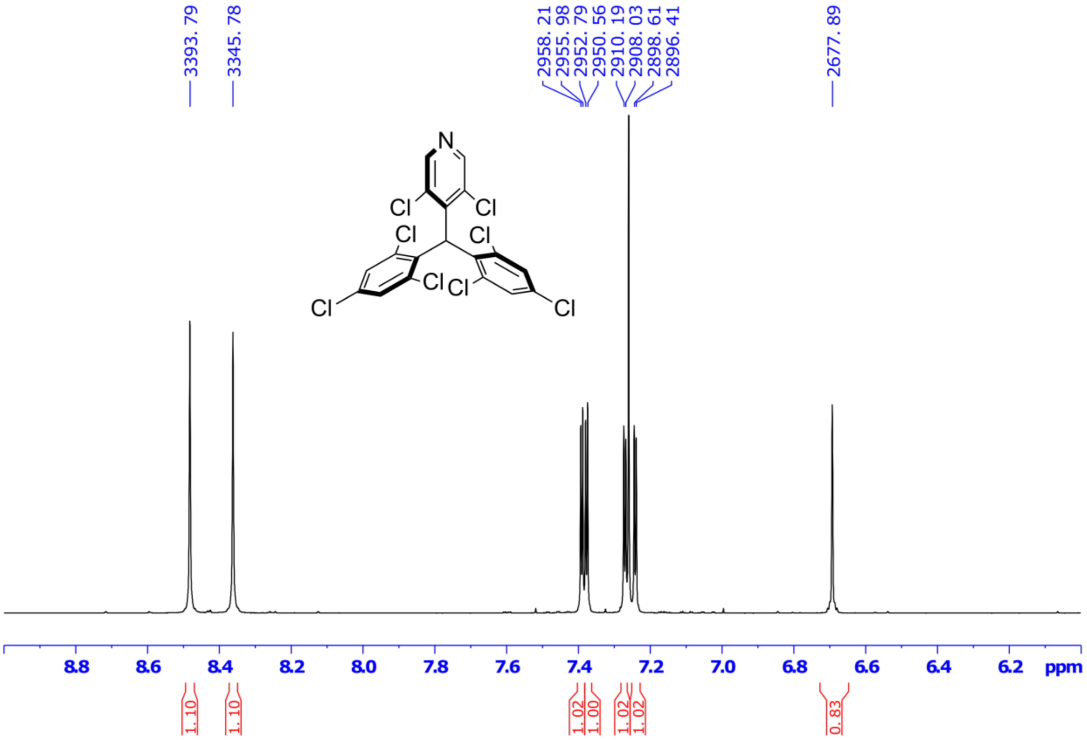

PyPBTM-H, ^{1}H NMR and ^{13}C NMR in CD_2Cl_2

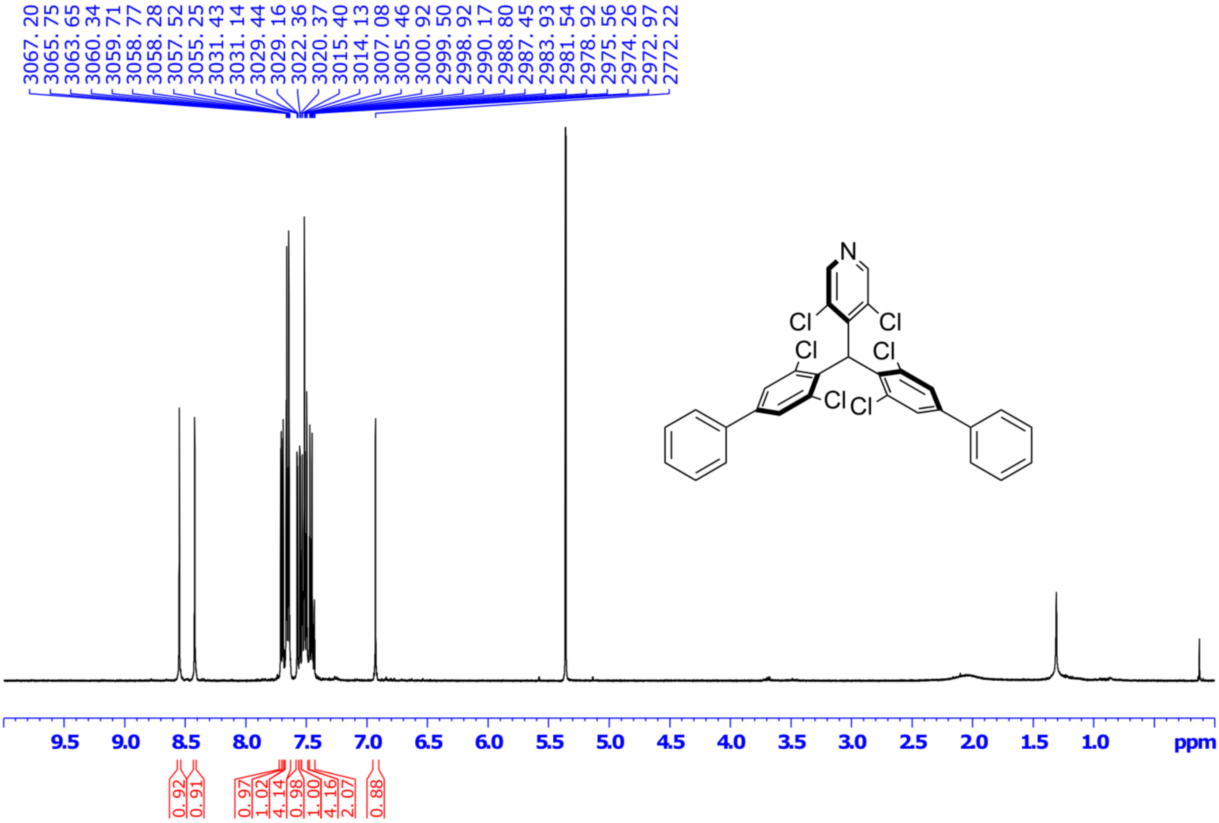

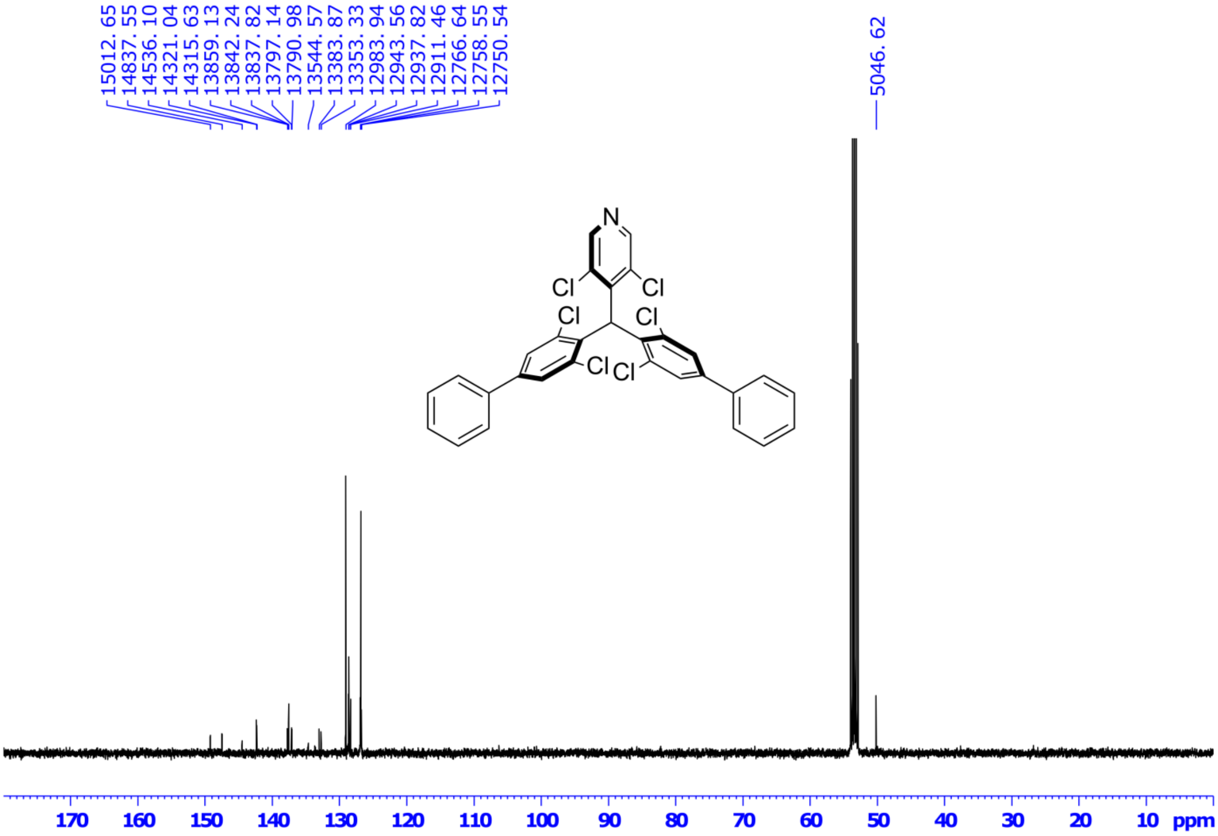

PyNBTM-H, ^{1}H NMR and ^{13}C NMR in CD_2Cl_2

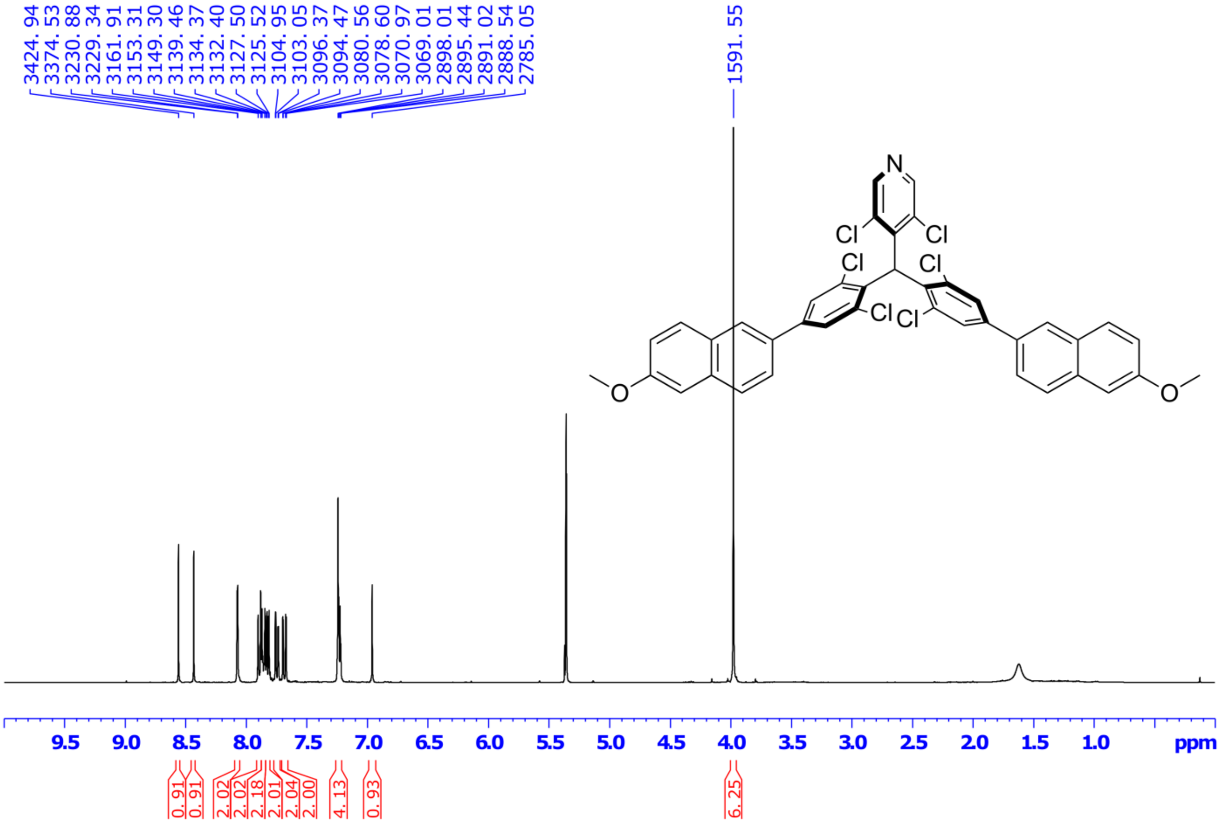

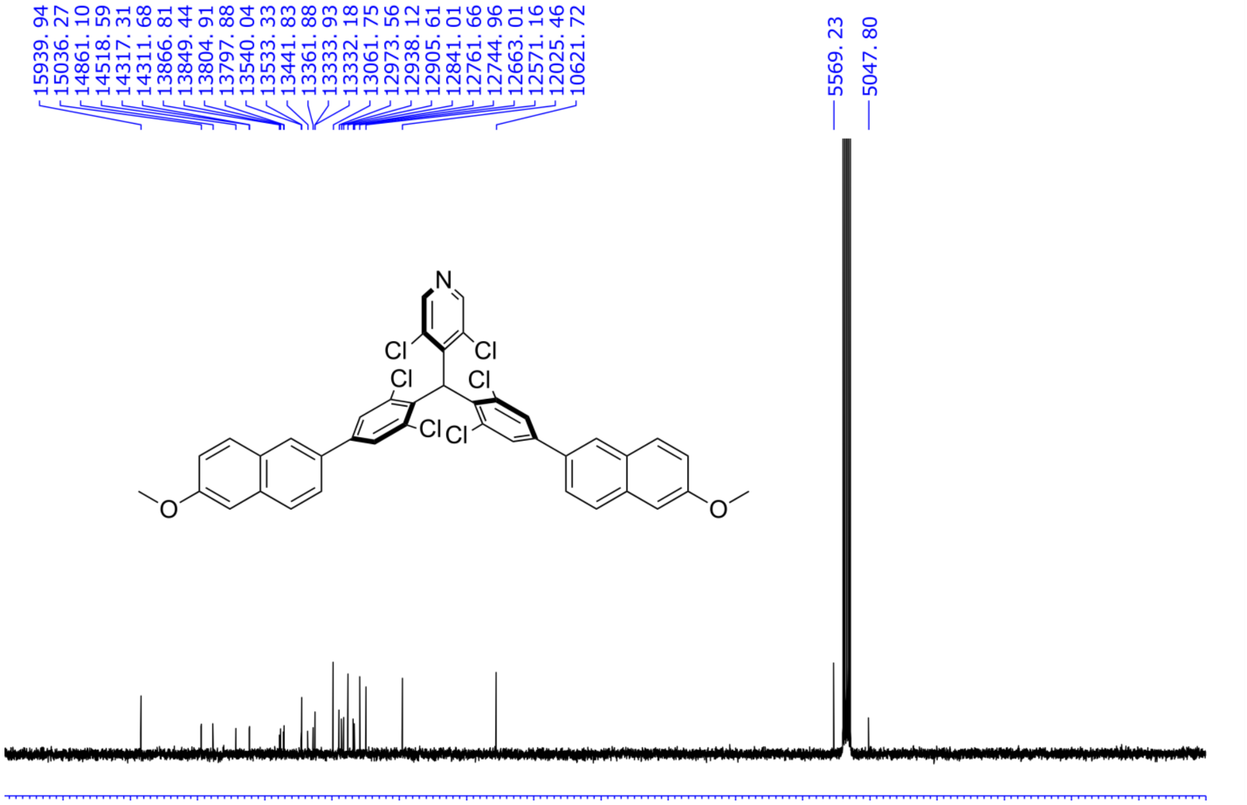

PyPhBTM-H, ^{1}H NMR and ^{13}C NMR in CD_2Cl_2

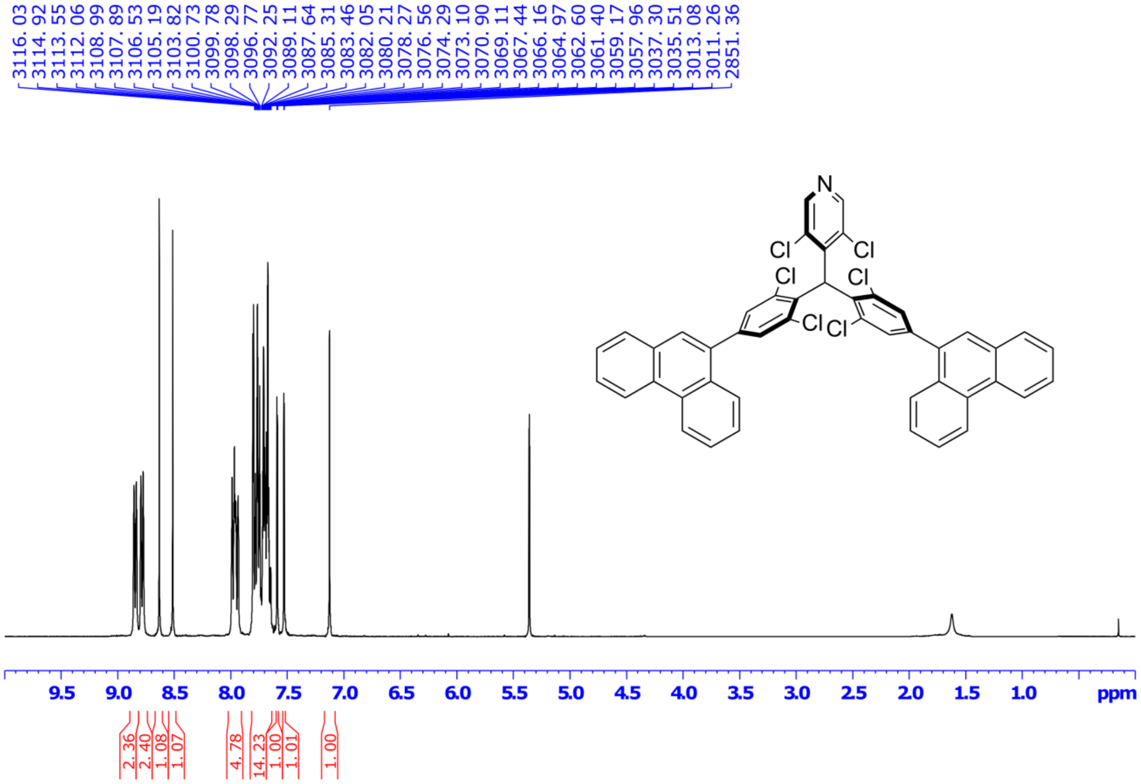

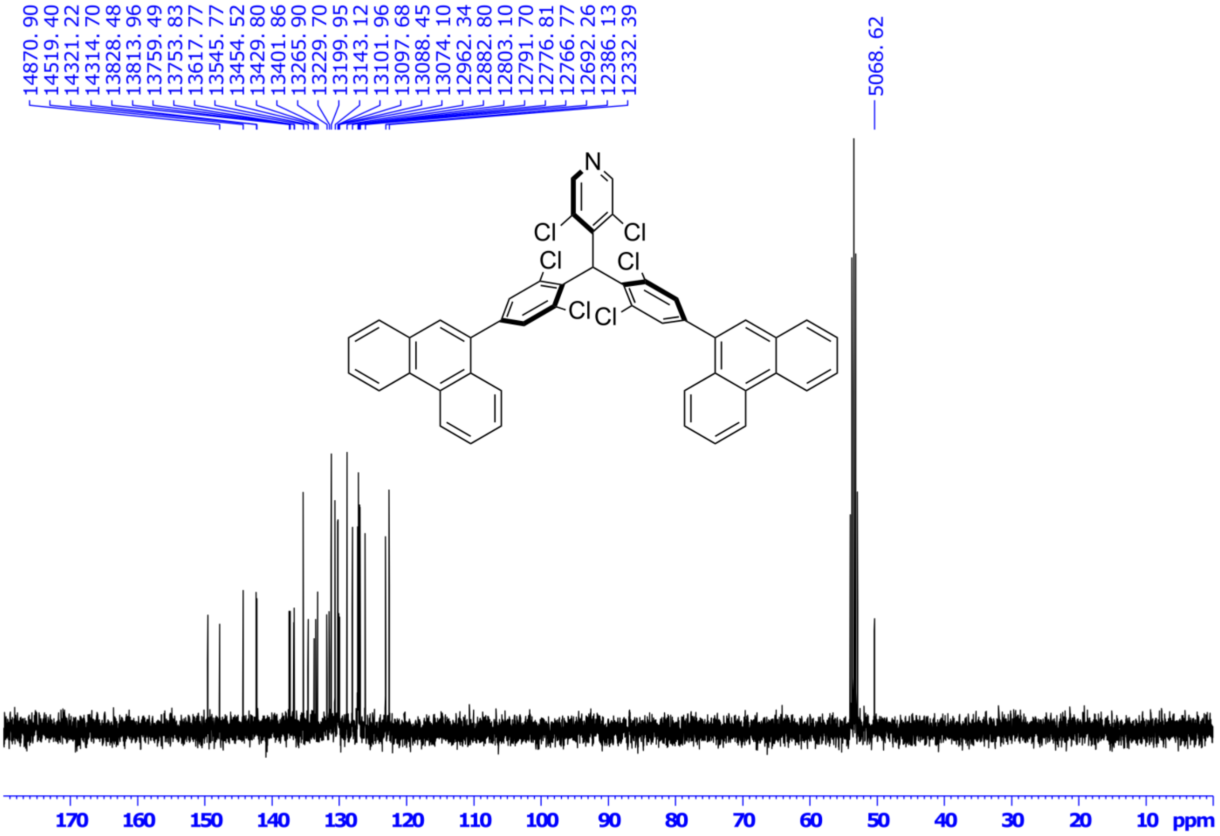

S11. ESR spectra of all radicals

PyPBTM, PyNBTM, and PyPhBTM in cyclohexane

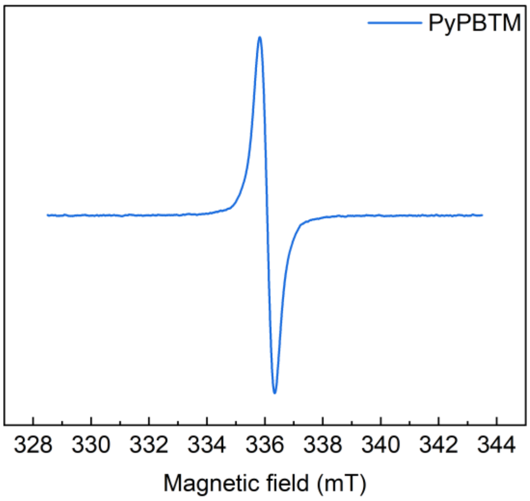

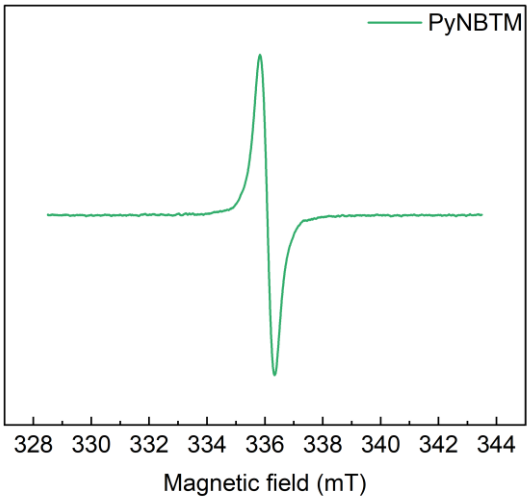

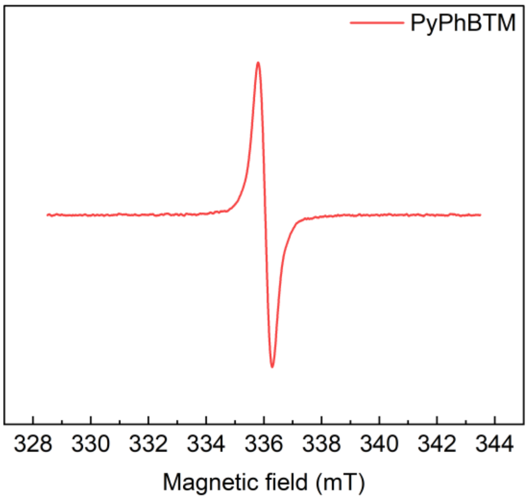

S12. Bibliography

1 Y. Hattori, T. Kusamoto and H. Nishihara, *Angew. Chemie - Int. Ed.*, 2014, **53**, 11845–11848.

2 C. Bannwarth, S. Ehlert and S. Grimme, *J. Chem. Theory Comput.*, 2019, **15**, 1652–1671.

3 S. Grimme, *J. Chem. Theory Comput.*, 2019, **15**, 2847–2862.

4 P. Pracht, F. Bohle and S. Grimme, *Phys. Chem. Chem. Phys.*, 2020, **22**, 7169–7192.

5 F. Neese, *WIREs Comput. Mol. Sci.*, 2012, **2**, 73–78.

6 F. Neese, *WIREs Comput. Mol. Sci.*, 2018, **8**, e1327.

7 A. Schäfer, H. Horn and R. Ahlrichs, *J. Chem. Phys.*, 1992, **97**, 2571–2577.

8 F. Weigend and R. Ahlrichs, *Phys. Chem. Chem. Phys.*, 2005, **7**, 3297–3305.

9 A. D. Becke, *J. Chem. Phys.*, 1993, **98**, 5648–5652.

10 S. Grimme, J. Antony, S. Ehrlich and H. Krieg, *J. Chem. Phys.*, 2010, **132**, 154104.

11 D. Alonso-Álvarez, D. Ross, E. Klampaftis, K. R. McIntosh, S. Jia, P. Storiz, T. Stolz and B. S. Richards, *Prog. Photovolt Res. Appl.*, 2015, **23**, 479–497.

12 V. I. Klimov, T. A. Baker, J. Lim, K. A. Velizhanin and H. McDaniel, *ACS Photonics*, 2016, **3**, 1138–1148.

13 B. Zhang, H. Yang, T. Warner, P. Mulvaney, G. Rosengarten, W. W. H. Wong and K. P. Ghiggino, *Methods Appl. Fluoresc.*, 2020, **8**, 037001.